Microscopic analysis of alpha scattering from ^{28}Si at 40 and 45 MeV

Subinit Roy, T. Dey, and A. Goswami
Saha Institute of Nuclear Physics, 1/AF, Bidhannagar, Calcutta 700 064, India

S. N. Chintalapudi and S. R. Banerjee
Variable Energy Cyclotron Centre, 1/AF, Bidhannagar, Calcutta 700 064, India
(Received 14 October 1991)

Angular distributions for the elastic and inelastic alpha scattering from ^{28}Si at $E_\alpha = 40$ and 45 MeV are analyzed in the framework of microscopic folding model. Transition densities are calculated from improved *s-d* shell-model wave functions and are also compared with those extracted from inelastic electron scattering data. The density-dependent Jeukenne-Lejeune-Mahaux interaction is used, besides the M3Y interaction, in an attempt to fit the large-angle data. Fairly good agreement with the data is obtained. The extracted M_n/M_p value for the 2^+ excited state of ^{28}Si also compares well with the shell-model prediction.

PACS number(s): 25.55.Ci

I. INTRODUCTION

The microscopic folding model was proposed as an alternative to the phenomenological description of the elastic scattering data to avoid the ambiguities [1] associated with the latter. Later it was extended to deformed folding model to describe the inelastic scattering events [2–4]. The basic ingredients in the deformed folding model are (i) the transition density, a quantity carrying all the nuclear structure informations, and (ii) an effective interaction fixed by the consistency requirement with the elastic scattering data. Because of its capacity of incorporate detailed structure informations and to bring out the transparent relationship between the *N-N* interaction and the nucleus-nucleus potential, the model has been found to be quite successful in describing the inelastic scattering data [5–11].

In this study a fully microscopic folding model analysis of inelastic scattering of α particle from the 2^+ (1.78 MeV) state of ^{28}Si at $E_\alpha = 40.0$ and 45.0 MeV is presented. The experiment was performed at Variable Energy Cyclotron Centre, Calcutta. The details of the experiment are given in Refs. [12] and [13].

Emphasis is given, primarily, in obtaining the transition density of the $0^+_{g.s.}$ to 2^+ (1.78 MeV) transition in ^{28}Si. The shell-model transition density with amplitudes obtained from the *s-d* shell calculation of Brown *et al.* [14] has been used. This nuclear structure calculation with the improved effective interaction [15] has proven very successful in describing electron scattering [14,16,17] and proton scattering at 200 to 400 MeV from ^{24}Mg and ^{28}Si [11]. But as far as we know, it has not been used in α scattering, an isoscalar probe, and is also rather strongly absorbed in the nucleus, unlike a proton. We therefore thought it worthwhile to test this in (α,α') scattering data. In addition to this, the proton transition density derived from the inelastic electron scattering [18] is also used. Then the neutron transition density for such an isoscalar transition in a nucleus with $N \approx Z$ is assumed to have the same shape. In the light of the α scattering, it would be interesting to observe the shell-model transition density in comparison with the model-independent transition density from the electron scattering data.

In the present analysis, we used the *g*-matrix-based M3Y interaction as one of the effective nucleon-nucleon interactions. The exchange effect that is important in this low-energy domain is included as a pseudopotential of zero range [8]. Being real in nature, the interaction yields only the real part of the nucleus-nucleus potential. It is energy independent and we did not consider the multiplicative factor to take into account the density-dependent effect [8,9]. Instead, along with the standard M3Y, we used the energy- and density-dependent effective interaction of Jeukenne, Lejeune, and Mahaux (JLM) [19]. Recently, Hogenbirk *et al.* [20] had indicated in their study of α scattering from ^{36}S at $E_\alpha = 36.61$ MeV that for low beam energy the JLM interaction may be more applicable than the standard M3Y. Good agreement with the data was also obtained by the same authors from proton scattering at $E_p = 28$ MeV [21] from ^{36}S. Unlike the M3Y, the JLM interaction is complex and generates both the real and imaginary components of the potential on folding.

For the sake of completeness, we used the same density-independent M3Y and density-dependent JLM interactions in the analysis of the elastic scattering data and obtained the "renormalization" factors often necessary for the folded potentials. The elastic scattering of alpha particle is a well known case where the α projectile, instead of being restricted only to the peripheral region, probes beyond the strong absorption radius producing the enhanced large-angle scattering. An attempt is also made to fit these data in the large-angle region in the microscopic model framework. The density dependence of the effective interaction accounts for the weak absorption in the interior and hence the density-dependent JLM interaction in comparison with the density-independent M3Y should give a better description of the large-angle

data. Normalization factors are determined from the overall fit to the data. Since the inelastic scattering selects the higher multipole components of the same interaction than the elastic, it provides a more consistent and stringent test of the interactions.

II. CALCULATION

The detailed procedure has been described in Refs. [22] and [23]. We will mention only the essential features of our calculation. The effective nucleon-nucleon interaction M3Y is employed in the form

$$V_{NN}(r_{12})=(\lambda_R+i\lambda_I)v_{NN}(r_{12}) , \tag{1}$$

where

$$v_{NN}(r_{12})=-262.0\delta(\mathbf{r}_{12})+\left[7999.0\frac{e^{-4.0r_{12}}}{4.0r_{12}}+2134.0\frac{3^{-2.5r_{12}}}{2.5r_{12}}\right] \tag{2}$$

is the "standard" energy- and density-independent form of the real M3Y interaction. The complex normalization factor is used to take into account the effect of the absorptive component of the optical potential. In this prescription it is tacitly assumed that the real and imaginary parts have similar range and shape.

To include the JLM interaction in the framework, the density, the energy, and the radial dependences of the effective nucleon-nucleon interaction may be written in a factorized form [24] as

$$v_{NN}=v(\rho_1,\rho_2,E)h(r_{12}) . \tag{3}$$

In our calculation we do not consider the projectile density (ρ_2) dependence of the interaction and use the isoscalar JLM interaction [19] in the improved local density approximation for $v(\rho_1,E)$. For the function $h(r_{12})$, the usual Gaussian form is used with a range $t=1.2$ fm. The energy E in Eq. (3) is actually the energy per nucleon of the projectile after the Coulomb energy is subtracted. As mentioned before, the JLM interaction is complex and following Hogenbirk *et al.* we assume that the imaginary part of the potential can also be generated by double folding. Because of low beam energy (≤ 50 MeV) and the large binding energy of the projectile alpha, breakup will not have any significant effect. According to Negele and Yazaki [25] the theoretical Im $v(\rho_1,E)$ is to be multiplied by the k-mass factor to include the effect of nonlocality. But in this low-energy domain ($E/A\sim 10$ MeV), as the nature of the experimental curve (Fig. 1 of Ref. [25]) suggests, this correction may not be necessary. Hence we use the folded imaginary potential without the nonlocality correction.

Before the two interactions are applied to inelastic scattering, to impose the consistency constraint, they are used to yield reasonably good fit to the elastic scattering data. The interactions, with the normalization factors thus obtained, are used to generate the transition potential. For the folded optical potential, the density of the projectile is taken to be Gaussian [8],

$$\rho_2(r_2)=0.4229\exp(-0.7024r_2^2) , \tag{4}$$

and a Fourier-Bessel expansion is used to obtain the ground-state density of the target ^{28}Si. The coefficients of the expansion are taken from Ref. [26] and the normalization is determined from the relation

$$\int\rho_1(r_1)d^3r_1=A . \tag{5}$$

The ground-state density is further unfolded to obtain the point-nucleon distribution.

The proton component of the total transition density

$$\rho_L(r)=\rho_L^p(r)+\rho_L^n(r) \tag{6}$$

is derived by unfolding the charge transition density obtained from the inelastic electron scattering [24]. Normalization is fixed by

$$M_p=\int\rho_L^p(r)r^{L+2}dr=[B(EL);J_i\rightarrow J_f]^{1/2} . \tag{7}$$

The charge transition matrix element $M_{\rm ch}=e\,M_p$ is taken to be 18.09 e fm^2 for $0^+_{\rm g.s.}$ to 2^+ (1.78 MeV) transition in ^{28}Si. The neutron transition density ρ_L^n is, however, assumed to have the same shape as the proton transition density ρ_L^p, an approximation often used for isoscalar transitions in many nuclei with $N\simeq Z$. Hence

$$\rho_L^n=N_n\rho_L^p , \qquad \rho_L=(1+N_n)\rho_L^p . \tag{8}$$

A direct consequence of this assumption is that the ratio of the neutron transition matrix element M_n to the proton transition matrix element M_p, i.e., M_n/M_p, is equal to N_n, the normalization constant determined by fitting the experimental cross section once the effective nucleon-nucleon interaction is properly chosen. We will present a comparison of the values of M_n/M_p obtained with the transition density from electron scattering and from the shell-model calculations.

The shell-model transition density is derived in the core plus valence nucleons approach. The valence contribution $A^{(i)}(r)$ ($i=p,n$) is calculated using the one-body density matrices (OBDM) tabulated by Brown *et al.* [14] (values given in isospin representation are converted to proton-neutron representation multiplying by a factor of $1/\sqrt{2}$). The details of the calculation are given in Ref. [10]. For the "core" transition density $C^{(i)}(r)$, which is to account for the effects of excitation of valence nucleons outside the model space as well as the polarization of the closed shells, we have chosen the shape to be the same as $A^{(i)}(r)$, so that

$$C^{(i)}(r)=N^{(i)}A^{(i)}(r) . \tag{9}$$

Hence the transition matrix elements become

$$M_i=\int(A^{(i)}+C^{(i)})r^{L+2}dr=(1+N^{(i)})M_i^v . \tag{10}$$

The valence transition matrices M_i^v are known from $A^{(i)}$. The core normalizations $N^{(i)}$ are evaluated using the

TABLE I. The volume integrals per nucleon and the rms radii of the real and imaginary components.

Energy (MeV)	Interaction	λ_R	λ_I	Volume integrals Real	Imaginary	rms rad (fm)	
40	M3Y	1.05	0.25	−426.92	−101.65	3.625	3.625
	JLM	0.90	1.00	−421.02	−103.02	3.910	4.131
45	M3Y	1.00	0.40	−406.59	−162.64	3.625	3.625
	JLM	0.90	1.00	−416.93	−108.39	3.912	4.148

effective charges $e_p, e_n = 1.35$ and 0.35 for valence protons and neutrons, respectively, for the quadrupole excitation in ^{28}Si, an *s-d* shell nucleus.

III. RESULTS AND DISCUSSION

The folded optical potentials with the M3Y and JLM interactions are presented in Fig. 1. The volume integrals per nucleon and the rms radii of the real and imaginary components are given in Table I. In the large *r* region, a region most sensitive to α scattering, the potential obtained with JLM interaction falls off more slowly compared to that obtained with the M3Y interaction. The elastic scattering fits obtained with these potentials are shown in Fig. 2. We note that the angular distribution calculated with JLM interaction does not fit the elastic scattering data well whereas an overall good fit is obtained with the M3Y interaction. The maxima and minima in the case of JLM interaction tend to shift inwards. The reason may be the greater diffuseness of the folded JLM interaction in the outer region. In Fig. 1(b) we also presented a plot of the imaginary potential for $E_\alpha = 45$ MeV which included the nonlocality correction of Negele and Yazaki. The use of this potential component yielded an angular distribution which considerably overestimated the data in the backward region without affecting much the data in the forward angle region. Hence in our final analysis we did not use this correction. The renormalization factors (λ_R, λ_I) needed for folded potentials are also shown in Table I. As expected, the normalizations for the real components (λ_R) of the M3Y and the JLM interactions and also the normalization for the imaginary component (λ_I) of the latter are close to unity. To maintain a consistency in the analysis the same set of λ_R and λ_I are used to generate the distorted waves for the inelastic scattering analysis.

The transition densities from inelastic electron scatter-

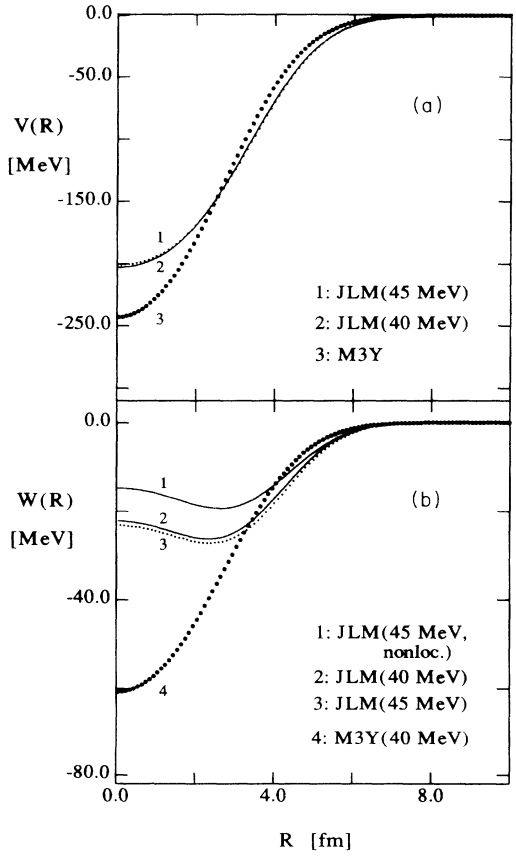

FIG. 1. Folded optical potentials with M3Y and JLM interactions. (a) Real potentials and (b) imaginary potentials for $E_\alpha = 40$ and 45 MeV. Curve in (b) represents the imaginary potential with the nonlocality correction for JLM interaction.

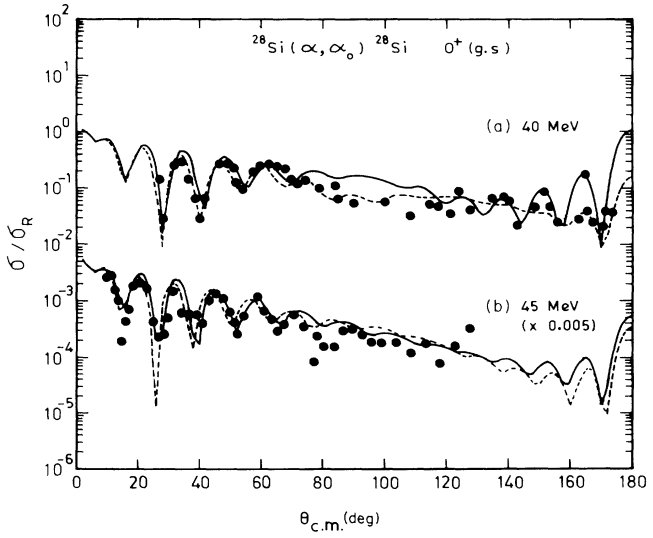

FIG. 2. Elastic scattering fits with the folded potentials. Microscopic fits (a) for 40 MeV and (b) for 45 MeV. The solid curve is with M3Y and the dotted curve is with JLM interaction. All the curves for $E_\alpha = 45$ MeV are scaled down by a factor of 0.005 for convenience in plotting.

ing and from shell-model calculations are shown in Fig. 3(a). The calculations utilize the shell-model results of Brown, Radhi, and Wildenthal (Table I, Ref. [11]). The single particle wave functions were determined using the Woods-Saxon shape potential with $V_0=-51.41$ MeV, $r_0=1.277$ fm, $a_0=0.362$ fm, $\lambda_{s.o.}=24.0$, $r_{s.o.}=1.1$ fm, and $a_{s.o.}=0.650$ fm, in an orbit-independent manner. Search is performed over the binding energies with the BOUND subroutine of code DWUCK4. With these wave functions for the valence shell the valence neutron and proton transition matrices are $M_n^{val}=10.1572$ fm^2 and $M_p^{val}=10.499$ fm^2. Taking into account the core contribution through the effective charges $e_p=1.35$ and $e_n=0.35$ the total neutron and proton transition matrices came about to be 17.3868 and 17.7286 fm^2, respectively. The real transition potentials are shown in Fig. 3(b). The potentials, obtained by folding the density-dependent JLM interaction, include the correction by Cheon *et al.* [27] that incorporates essentially a dynamic dependence on density for the transition potential. With this correction the imaginary transition potential with the JLM interaction, having a node in its radial shape, differs vastly from the others. In spite of this difference, the quantitative nature of the agreement with the data improved significantly and both the models now yield more-or-less similar angular distribution.

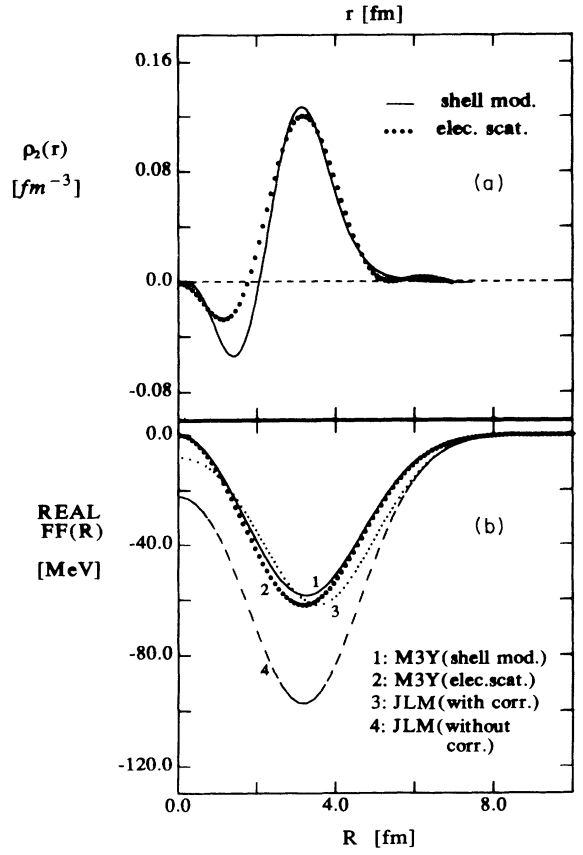

FIG. 3. (a) Transition densities for 2^+ (1.78 MeV) state of ^{28}Si. (b) The real form factors with M3Y and JLM interactions for $E_\alpha=45$ MeV. Curves 3 and 4 of (b) are form factors with and without Cheon correction, respectively.

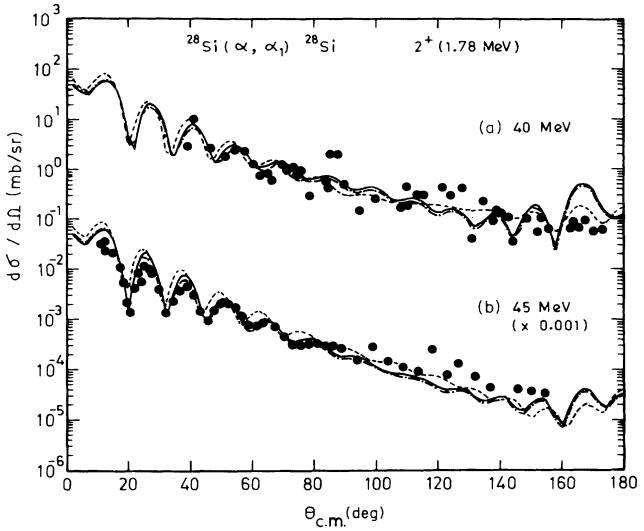

FIG. 4. Differential cross-section data for the 1.78 Mev 2^+ state of ^{28}Si (a) for 40 MeV and (b) for 45 MeV. The solid and dash-dotted curves are with M3Y interaction using the shell-model and the macroscopic [from (e,e') data] transition densities, respectively. The dotted curve is with JLM interaction using the shell-model transition density. All the curves for 45 MeV are scaled down by 0.001 for convenience.

The differential cross sections for inelastic scattering to 2^+, 1.78 MeV state have been presented in Fig. 4. Good fits are obtained with the fully microscopic calculations. Though like the elastic scattering description here also it is observed that with the density-dependent JLM interaction the distributions tend to shift inward. In the backward angle region ($\theta_{c.m.}\geq 90°$), the fit obtained with JLM interaction for $E_\alpha=40$ MeV is slightly better compared to the calculated angular distribution with M3Y interaction. For $E_\alpha=45.0$ MeV, in the large-angle region, none of the calculated angular distributions fit the data well. While the angular distribution with the JLM interaction overestimates the data, that with the M3Y underestimates it.

The isoscalar transition strength $M_0=M_n+M_p$, which gives a measure of the strength of the transition, and the ratio M_n/M_p are determined form the distorted wave Born approximation fit to the data with the transition density from the (e,e') form factor. The fitted density gives $M_0=35.456$ fm^2 and hence $N_n=M_n/M_p=0.96$. The shell-model calculation predicts $M_0=35.11$ fm^2 and the ratio $M_n/M_p=0.98$. The qualitative agreement between the shell-model prediction and the fitted value is quite good, assigning greater confidence in the analysis and the shell-model wave functions of Brown and Wildenthal for the low-lying quadrupole states.

IV. CONCLUSION

A fully microscopic calculation of α scattering from ^{28}Si at 40.0 and 45.0 MeV with a density- and energy-independent effective interaction (M3Y) and a density-

and energy-dependent interaction (JLM) was attempted. Our primary interests were twofold: firstly, to see how far a microscopic calculation can describe the angular distribution data that extend up to a very large angle, and secondly, to test the shell-model transition density in comparison with the density from the (e,e') data that can be used directly in the microscopic framework to generate the transition potential. Two types of effective interactions were used to make our inferences independent of the nature of the interactions. Following the consistency condition the same folded interactions which described the elastic scattering data quite well were used to generate the distorted waves for the inelastic scattering. We also derived the isoscalar transition strength M_0 and the ratio M_n/M_p from the fit and compared with the shell-model predictions.

It is observed that good quality fits are obtained in the microscopic framework with both the density-dependent and -independent effective interactions. This indicates that the microscopic prescription can be successfully employed to describe the low-energy α-scattering data. The improved *s-d* shell wave functions with correct radial fall-off, as tested by the scattering of alpha particles, describe the structure of the low-lying 2^+ state of ^{28}Si well, a view also supported by (e,e') and (p,p') scattering data.

We thank Dr. S. K. Datta, presently at Nuclear Science Centre, JNU, New Delhi, for the valuable discussions we had with him at different stages of this work.

[1] G. Igo, Phys. Rev. Lett. **1**, 72 (1958); Phys. Lett. **74B**, 202 (1978).
[2] N. K. Glendenning and M. Veneroni, Phys. Lett. **14**, 228 (1965); Phys. Rev. **144**, 839 (1966).
[3] G. R. Satchler, Nucl. Phys. **77**, 481 (1966); Nucl. Phys. **A95**, 1 (1967).
[4] D. F. Jackson and V. K. Kembhavi, Phys. Rev. **178**, 1626 (1969).
[5] A. M. Kobos, B. A. Brown, R. Lindsay, and G. R. Satchler, Nucl. Phys. **A425**, 205 (1984).
[6] R. Pesl, H. J. Gils, H. Rebel, E. Friedmann, J. Buschmann, H. Klewe-Nebenius, and S. Zargromski, Z. Phys. A **313**, 111 (1983).
[7] S. K. Datta, Subinit Ray, H. Mazumdar, S. K. Ghosh, C. Samanta, S. Roy, P. Dasgupta, S. N. Chintalapudi, and S. R. Banerjee, Phys. Rev. C **39**, 1281 (1989).
[8] G. R. Satchler and W. G. Love, Phys. Rep. **55**, 183 (1979).
[9] D. K. Srivastava and H. Rebel, Z. Phys. A **316**, 225 (1984); J. Phys. G **10**, L127 (1984).
[10] Subinit Roy and S. K. Datta, Phys. Rev. C **44**, 912 (1991).
[11] K. Hicks *et al.*, Phys. Rev. C **38**, 229 (1988).
[12] Tarun Dey *et al.*, in *Proceedings of the International Conference on Direct Nuclear Reactions, Bangalore, India, 1989,* edited by N. G. Puttaswamy (World Scientific, Singapore, 1991).
[13] V. P. Darshan, Ph.D. thesis, Bangalore University, 1991.
[14] B. A. Brown, R. Radhi, and B. H. Wildenthal, Phys. Rep. **101**, 313 (1983).
[15] B. H. Wildenthal, Bull. Am. Phys. Soc. **27**, 725 (1982).
[16] M. Carchidi *et al.*, Phys. Rev. C **34**, 2280 (1986).
[17] S. Yen *et al.*, Phys. Lett. **124B**, 471 (1983).
[18] R. P. Singhal *et al.*, Nucl. Phys. **A323**, 91 (1979).
[19] J. P. Jeukenne, A. Lejeune, and C. Mahaux, Phys. Rev. C **16**, 80 (1977).
[20] A. Hogenbirk *et al.*, Phys. Lett. B **223**, 282 (1989).
[21] A. Hogenbirk *et al.*, Nucl. Phys. **A516**, 205 (1990).
[22] G. R. Satchler, *Direct Nuclear Reactions* (Oxford University Press, New York, 1983).
[23] G. R. Satchler, Nucl. Phys. **A472**, 215 (1987).
[24] F. Petrovich *et al.*, Phys. Lett. **71B**, 259 (1977).
[25] J. W. Negele and K. Yazaki, Phys. Rev. Lett. **47**, 71 (1981).
[26] H. De Vries *et al.*, At. Data Nucl. Data Tables **36**(3), 495 (1987).
[27] T. Cheon, K. Takayanagi, and K. Yazaki, Nucl. Phys. **A437**, 301 (1985).